Supporting Online Material for

Control of Graphene's Properties by Reversible Hydrogenation: Evidence for Graphane

D. C. Elias,[1] R. R. Nair,[1] T. M. G. Mohiuddin,[1] S. V. Morozov,[2] P. Blake,[3] M. P. Halsall,[1] A. C. Ferrari,[4] D. W. Boukhvalov,[5] M. I. Katsnelson,[5] A. K. Geim,[1,3] K. S. Novoselov[1]*

To whom correspondence should be addressed. E-mail: kostya@manchester.ac.uk

This PDF file includes:

SOM Text

Figs. S1 to S7

References

Supplementary Online Material

"Control of graphene's properties by reversible hydrogenation" by D. C. Elias *et al*

SUPPLEMENTARY TEXT

1. Non-uniform Hydrogenation of Graphene Membranes

In the main text, we described graphane crystals exhibiting lattice periodicity *d* notably shorter than that in graphene. We have observed a range of *d* values rather than a single period expected for homogenous graphane. This was attributed to the inevitable mechanical strain induced when parts of the crystal rigidly attached to a metal scaffold had to shrink during conversion of graphene into graphane (its adhesion to an evaporated metal is expected to be very strong as graphene deposited on plastic can already sustain strains of > 1% *(S1)*). To minimize the effect of strain, we chose to work with partially broken membranes that allowed at least a part of the strain to relax due to the presence of free boundaries.

To emphasize the importance of strain effects, here we describe in addition what happens in the extreme case when a graphene membrane has no free boundaries. Figure S1A shows a TEM micrograph of a hydrogenated crystal that completely covers a 50 μm aperture in a 15 μm thick copper film *(S2)*. For this membrane, we observed not only the regions that contracted but also those that drastically expanded. The former exhibited *d* down to 2.37 ±0.02 Å (i.e. 4% smaller than in graphene), in agreement with the results for partial and ruptured membranes reported in the main text. In the expanded regions, *d* could be as large as ≈2.7 Å (i.e. the lattice was stretched isotropically by nearly 10% with respect to pristine graphene). Figure S1B shows an example of such an extremely stretched graphene lattice. One can see that the diffraction spots occur inside the red hexagon indicating the diffraction pattern in graphene, which is directly opposite to Fig. 4A that shows the same diffraction spots but outside the red hexagon. This amount of stretching is close to the limit of possible elastic deformations in graphene *(S3)* and, indeed, we observed some of our membranes to rupture during their hydrogenation. We believe that the stretched regions are likely to remain non-hydrogenated.

It is hardly surprising that if a part of a rigidly fixed membrane shrinks, other parts have to extend. However, we found that instead of exhibiting random stretching, graphene membranes normally split into domain-like regions. The symmetry within each domain remained hexagonal

but with either increased or decreased *d*. In other words, not only contraction due to hydrogenation was isotropic (as already discussed in the main text) but also the expansion was mostly isotropic. Having said that, we also observed expanded regions, for which the hexagonal diffraction pattern was stretched along some preferential direction (usually, a crystallographic one) and the diffraction spots were blurred. Analysis of many diffraction images revealed that a typical domain size was of the order of 1 µm and the uniaxial part of strain was significantly smaller than its isotropic component and never exceeded ≈2%. The annealing of membranes (without free boundaries) also led to complete recovery of the original periodicity in both stretched and compressed domains.

2. Binding of Hydrogen to Ripples

In the main text, we have presented a simple argument that atomic hydrogen should preferentially bind to apexes of corrugated graphene due to a contribution from elastic energy. However, there is also a contribution from the electronic energy which works in parallel and promotes the local bonding of atomic hydrogen. The electronic structure of a non-hydrogenated curved graphene is characterized by the appearance of so-called mid-gap states *(S4)* (see the red curve in Figure S2). Our numerical simulations show that the attachment of a pair of hydrogen atoms leads to the splitting of the mid-gap peak, leading to the formation of symmetric (donor and acceptor) quasi-localized states (blue curve). For denser hydrogen coverage, an energy gap opens in the electronic spectrum of rippled graphene (green curve). One can see that the splitting moves the mid-gap states away from zero energy, leading to a gain in total energy. This mechanism seems to be rather general: humps in graphene can stabilize themselves by catching impurity states, and also favours hydrogenation of convex regions.

3. Estimate for the Energy Gap Induced by Hydrogenation of Graphene on Substrate

The notion of preferential hydrogenation of humps on a graphene surface can be combined with the concept of graphene sheets being generally rippled *(S5,S6,S7)*. The combination leads to the following scenario for the disordered chemical derivative obtained by single-sided hydrogenation. This derivative is likely to consist of two phases: convex regions decorated with hydrogen and concave areas that remain non-hydrogenated (see Fig. 3A). In the hydrogenated regions, carbon atoms acquire sp^3 hybridisation and an energy gap opens, whereas non-

hydrogenated regions retain their sp^2 metallic character (see the calculations in Fig. S2). The corresponding electronic spectra are schematically shown in Fig. S3B.

The two-phase picture allows a rough estimate for the energy gap in the hydrogenated convex regions. To this end, we assume that at the neutrality point the metallic concave regions are well separated by the gapped regions so that the system as a whole is insulating. By applying gate voltage, we add charge carriers that fill in the localized states in the gapped regions and the Dirac cones in the metallic ones (see Fig. S3B,C). Eventually, the Fermi level reaches the bottom (top) of the conduction (valence) in the hydrogenated regions, thus bringing the whole system into the metallic regime. Experimentally, this occurs at $n \approx 4 \times 10^{12}$ cm^{-2} (see the main text), which corresponds to a shift of the Fermi energy by ~0.25eV. This yields an energy gap of ~0.5eV for the single-sided hydrogenation. This estimate provides a lower bound for the energy gap as it neglects a contribution from the localised states, quantum confinement effects and a smaller capacitance to the gate for the case of microscopic regions.

To explore the nature of the insulating state of single-sided graphane we measured its *I-V* characteristics (Fig. S4). They have exhibited strongly non-linear behaviour, in contrast to the case of graphene. The level of non-linearity varies with carrier concentration, and the curves become practically linear for carrier concentrations above ~5×10^{12} cm^{-2}, which further supports our conclusions above and in the main text. The nonlinearity disappears with increasing *T* (Fig. S4; inset), with conductivity at zero bias following the $\exp[-(T_0/T)^{1/3}]$ dependence.

4. Mass Spectrometry of Gas Desorption from Hydrogenated Graphene

To confirm the presence of hydrogen on the surface of graphene after its hydrogenation, we performed mass-spectrometry of gases desorbed from its surface during thermal annealing. To this end, we started with a graphene suspension in DMF (dimethylformamide), which was prepared by ultrasonic exfoliation (*S8,S9)* of natural graphite flakes (*S10*). SiO$_2$/Si wafers were then spin-coated using this suspension, which resulted in uniform thin films consisting of overlapping submicron flakes of graphene. They were then exposed to the hydrogen-argon plasma for 2 hours. After hydrogenation the samples were heated up to 350°C in vacuum while the atmosphere in the chamber was monitored by a mass-spectrometer. The observed intermittent flow of hydrogen (Fig. S5) clearly proves that it gets adsorbed at the surface of graphene even during single-sided hydrogenation and can then be desorbed by modest heating. In a control

experiment, we used samples prepared in parallel with those measured in Fig. S5 but exposed only to pure argon plasma under the same conditions. The control samples exhibited a significantly lower hydrogen signal attributed to desorption of water from heated surfaces (Fig. S5).

5. Corrugation of Hydrogenated Graphene

We have also performed electron diffraction studies of hydrogenated graphene membranes in a tilted geometry (*S5,S6*). The blurring of diffraction spots provides information about the flatness of the membranes (*S5,S6*). The hydrogenated membranes that exhibited only a slightly shorter lattice periodicity showed the same level of corrugation as pristine graphene (Fig. S6A,B,E). On the other hand, those membranes that had a strongly compressed lattice showed significantly lower corrugations (Fig. S6C,D,E).

The broadening of the diffraction peaks at zero tilt provides the information about the uniformity of our samples. This broadening for hydrogenated graphene was found to be very similar to that in pristine graphene, which indicates that our membranes were uniformly hydrogenated (at least over the areas used for the electron diffraction – 0.3μm). The probable reason for the uniform hydrogenation is high mobility of hydrogen atoms along the surface (*S11*), which allows them to achieve the lowest energy configuration characteristic of graphane.

6. Hydrogenation of Bilayer Graphene

We have applied our hydrogenation procedures also to bilayer graphene. Bilayer samples on a substrate exhibited significantly lower affinity to hydrogen as revealed in measurements of their Raman spectra and transport characteristics. Bilayer samples showed little change in their charge carrier mobility and only a small D peak, as compared to single-layer graphene exposed to the same hydrogenation procedures (Fig. S7).

This observation is in agreement with the theory that hydrogen cannot be adsorbed on one side of a flat graphene surface and our conclusions that hydrogen adsorption for graphene on a substrate is facilitated by ripples (see above). We believe that higher rigidity of bilayers suppresses their rippling *(S5,S6)*, thus reducing the probability of hydrogen adsorption.
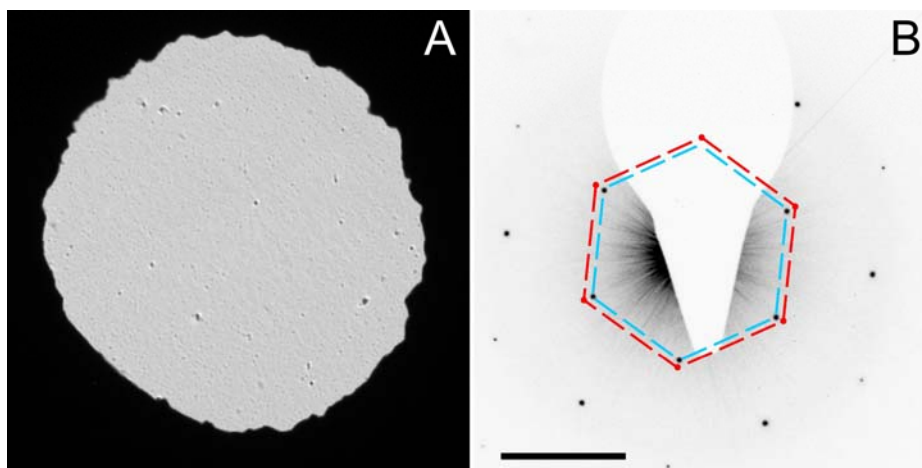
Figure S1. (A) - TEM micrograph of one of our graphene membranes without free boundaries. The presence of a graphene crystal covering the whole aperture is evidenced only by some particulate in the image. (B) - Changes in the lattice constant after extended exposure of this membrane to atomic hydrogen. The scale bar is 5 nm^{-1}. The diffraction pattern is for an unusual case of a region with a strongly stretched lattice ($d \approx 2.69$ Å). The beam diameter used for selected area electron diffraction is 0.3 μm. The blue hexagon is a guide to the eye and marks the positions of the diffraction spots. The equivalent spots in unstrained graphene under the same conditions are shown by the red hexagon and dots.
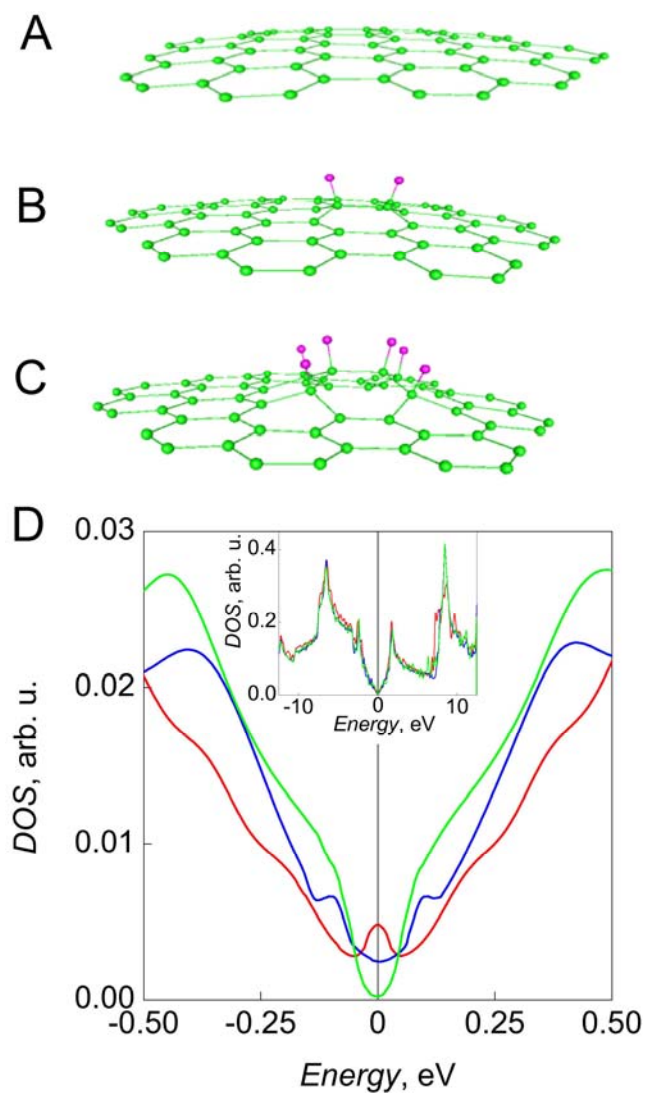
Figure S2. Convex graphene sheet with none (A), two (B) and six (C) hydrogen atoms adsorbed. Atomic coordinates for (B) and (C) were optimized using density functional calculations with the SIESTA code. Configuration (A) was deduced from (B) by removing hydrogen atoms and eliminating the excess displacement for the two carbon atoms that bound hydrogen. (A) corresponds to a ripple of diameter 1.07 nm and height 0.094 nm. (D) – Electronic density of states for configurations A, B and C (red, blue and green curves, respectively). The mid-gap state at zero energy (A; red) becomes split due to adsorption of two hydrogen atoms (B; blue) and a gap opens if more atoms are attached (C; green). Inset: Same calculations for a wider energy range.
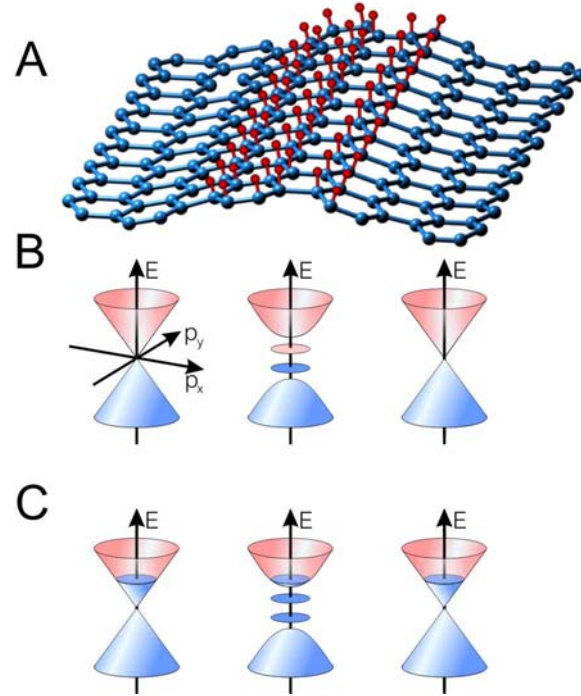
Figure S3. Metal-insulator transition in the disordered graphene derivative obtained by single-sided hydrogenation. (A) – Two-phase model for this derivative: hydrogenated convex regions are adjoined by non-hydrogenated concave ones. Blue (red) spheres represent the carbon (hydrogen) atoms. (B) – Schematic band diagrams for the two phases shown in (A). The diagrams are positioned under the corresponding graphene regions. Hydrogenated regions are represented by a gapped spectrum whereas the concave regions are assumed to be gapless (these are simplified versions of the spectra shown by the red and green curves Fig. S2D). The occupied (unoccupied) states are indicated by blue (pink). The ellipsoids inside the gap represent localised states. The Fermi level in (B) is at the neutrality point. (C) – Same as (B) but the system is doped by electrons so that the Fermi level reaches the bottom of the conductance band in the hydrogenated region.
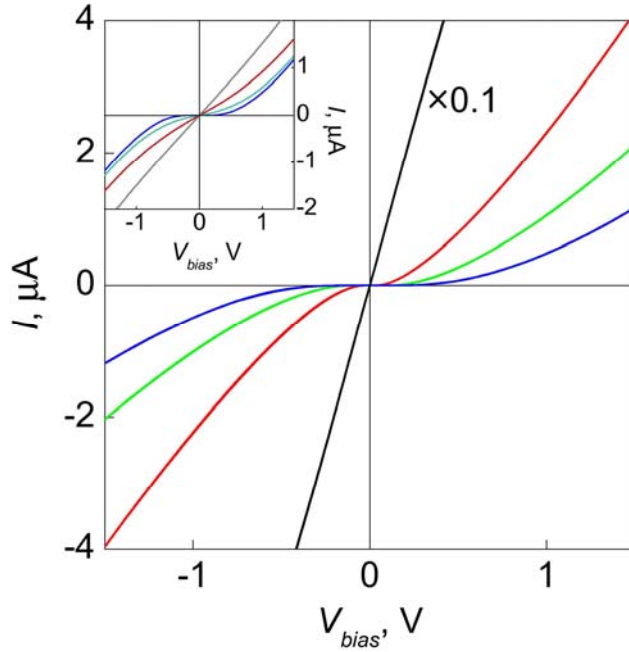
Figure S4. *I-V* characteristics of a hydrogenated graphene sample; *T*=2.5K. The blue curve is taken at the neutrality point (V_g = 47V, see Fig. 1C of the main text); green – at a hole concentration of $\approx 1.5 \times 10^{12}$ cm^{-2}; red – hole concentration $\approx 3 \times 10^{12}$ cm^{-2} (carrier concentrations are estimated from the device capacitance and applied gate voltage). The black curve is for the hydrogenated device after its thermal annealing at the neutrality point (note the difference in scales). *I-V* characteristics for pristine graphene practically coincide with the black curve. Inset: Temperature dependence of the *I-V* characteristics at the neutrality point for hydrogenated graphene. From bottom to top: *T* = 2.5K; 40K; 80K; 160K.
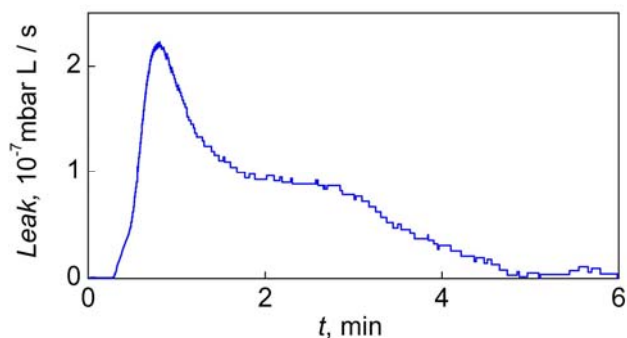
Figure S5. Desorption of hydrogen from single-sided graphane. The measurements were done by using a leak detector tuned to sense molecular hydrogen. The sample was heated to 300°C (the heater was switched on at $t = 10$s). Control samples (exposed to pure argon plasma) exhibited much weaker and featureless response ($<5 \times 10^{-8}$ mbar L/s), which is attributed to desorption of water at heated surfaces and subtracted from the shown data (water molecules are ionized in the mass-spectrometer, which also gives rise to a small hydrogen signal).
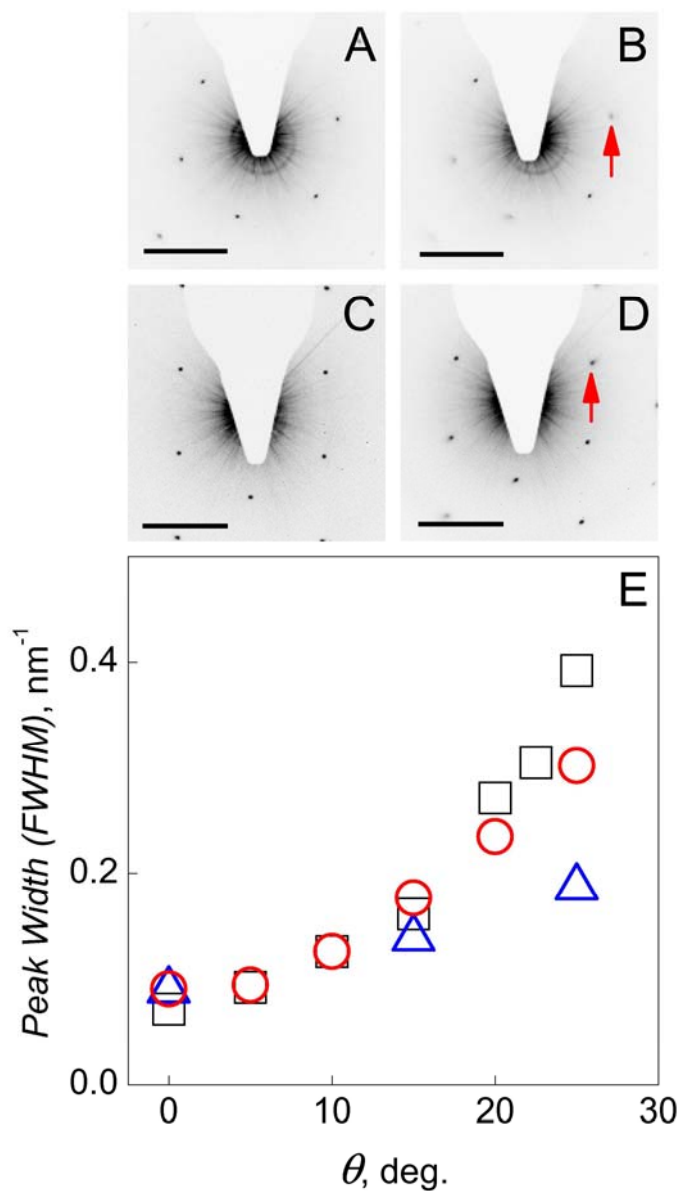
Figure S6. Broadening of (0-110) electron diffraction peaks in graphane. A (B) – Region of hydrogenated graphene with $d \approx 2.42$ Å; tilt angle is 0° (15°). Note the strong blurring of the (0-110) diffraction spot (marked by the red arrow). C (D) – Region with $d \approx 2.35$ Å; tilt angle is again 0° (15°). The broadening of the same spot is smaller than in B. E – broadening of the (0-110) diffraction peak as a function of tilt angle θ. Black squares indicate pristine graphene; red circles hydrogenated graphene with $d \approx 2.42$ Å; and blue triangles graphane ($d \approx 2.35$ Å).
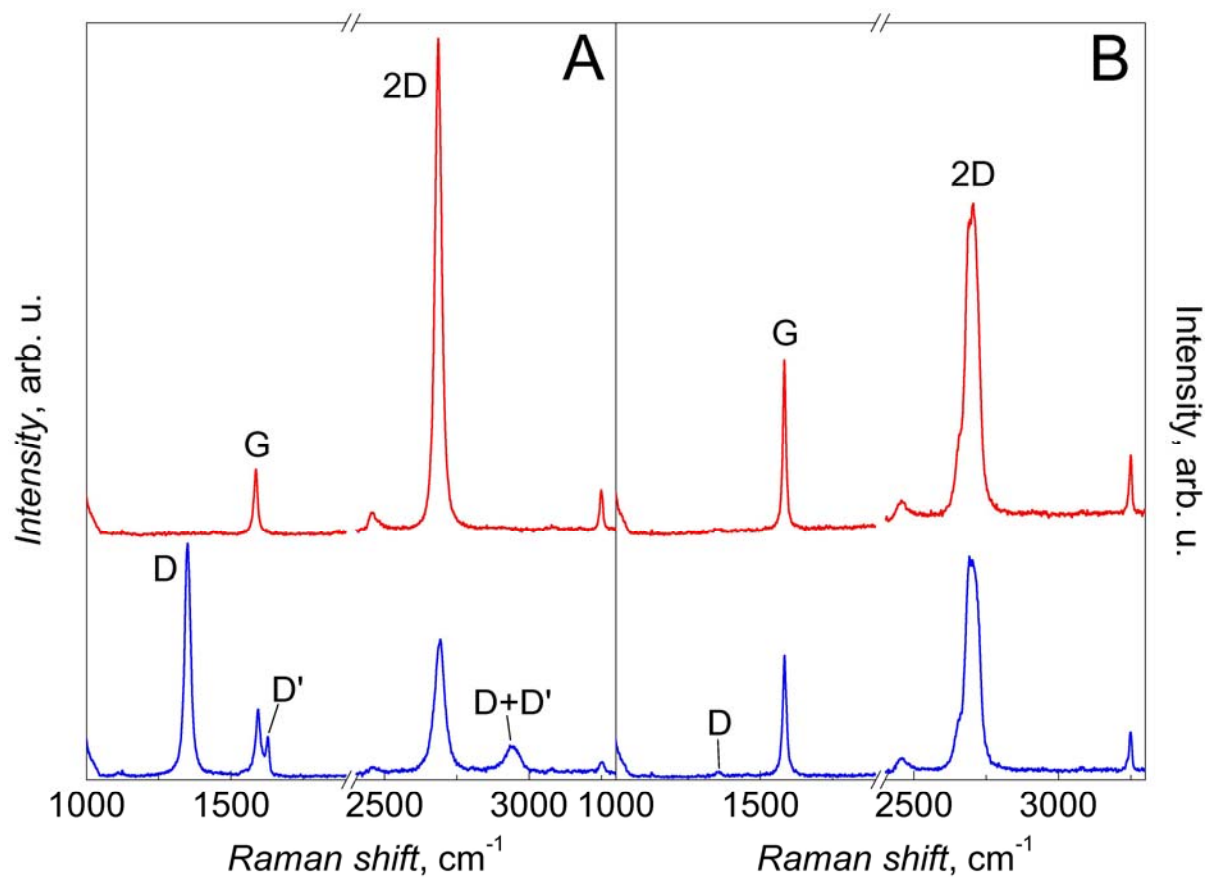
Figure S7. Changes in Raman spectra of single-layer (A) and bilayer graphene (B) induced by hydrogenation. Both samples were on the same SiO_2/Si wafer and were hydrogenated simultaneously for 2 hours. Red and blue curves correspond to pristine and hydrogenated samples, respectively. The spectra were measured with a Renishaw spectrometer at a wavelength of 514 nm and using low power to avoid graphene's damage during measurements.

SUPPLEMENTARY REFERENCES

[s1] Zhen Hua Ni *et al.*, arXiv:0810.3476.

[s2] T. J. Booth *et al.*, *Nano Lett.* **8**(8), 2442-2446 (2008).

[s3] C. Lee, X.ei, J. W. Kysar, J. Hone, *Science* **321**, 385 – 388 (2008).

[s4] F. Guinea, M. I. Katsnelson, M. A. Vozmediano, *Phys. Rev. B* **77**, 075422 (2008).

[s5] J. C. Meyer *et al.*, *Nature* **446**, 60-63 (2007).

[s6] J. C. Meyer *et al.*, *Solid State Commun.* **143,** 101-109 (2007).

[s7] E. Stolyarova *et al., Proc. Natl Acad. Sci. USA* **104,** 9209-9212 (2007).

[s8] P. Blake *et al., Nano Letters* **8**(6) 1704 – 1708 (2008).

[s9] Y. Hernandez *et al., Nature Nanotech.* **3**, 563 - 568 (2008).

[s10] www.grafite.com

[s11] J. C. Meyer *et al.*, *Nature* **454**, 319 - 322 (2008).